WILEY **gebiology**

A case study for late Archean and Proterozoic biogeochemical iron- and sulphur cycling in a modern habitat—the Arvadi Spring

Elif Koeksoy[1] | Maximilian Halama[1] | Nikolas Hagemann[1] | Pascal R. Weigold[1] | Katja Laufer[1,2] | Sara Kleindienst[1] | James M. Byrne[1] | Anneli Sundman[1] | Kurt Hanselmann[3] | Itay Halevy[4] | Ronny Schoenberg[5] | Kurt O. Konhauser[6] | Andreas Kappler[1,2] (iD)

[1]Geomicrobiology, Center for Applied Geosciences, University of Tuebingen, Tuebingen, Germany

[2]Bioscience, Center for Geomicrobiology, Aarhus University, Aarhus, Denmark

[3]Geological Institute, ETH Zuerich, Zuerich, Switzerland

[4]Earth and Planetary Sciences, Weizmann Institute of Science, Rehovot, Israel

[5]Isotope Geochemistry, University of Tuebingen, Tuebingen, Germany

[6]Earth and Atmospheric Sciences, University of Alberta, Edmonton, AB, Canada

Correspondence
Andreas Kappler, Geomicrobiology, Center for Applied Geosciences, University of Tuebingen, Sigwartstrasse 10, D-72076 Tuebingen, Germany.
Email: andreas.kappler@uni-tuebingen.de

Abstract

As a consequence of Earth's surface oxygenation, ocean geochemistry changed from ferruginous (iron(II)-rich) into more complex ferro-euxinic (iron(II)-sulphide-rich) conditions during the Paleoproterozoic. This transition must have had profound implications for the Proterozoic microbial community that existed within the ocean water and bottom sediment; in particular, iron-oxidizing bacteria likely had to compete with emerging sulphur-metabolizers. However, the nature of their coexistence and interaction remains speculative. Here, we present geochemical and microbiological data from the Arvadi Spring in the eastern Swiss Alps, a modern model habitat for ferro-euxinic transition zones in late Archean and Proterozoic oceans during high-oxygen intervals, which enables us to reconstruct the microbial community structure in respective settings for this geological era. The spring water is oxygen-saturated but still contains relatively elevated concentrations of dissolved iron(II) (17.2 ± 2.8 μM) and sulphide (2.5 ± 0.2 μM) with simultaneously high concentrations of sulphate (8.3 ± 0.04 mM). Solids consisting of quartz, calcite, dolomite and iron(III) oxyhydroxide minerals as well as sulphur-containing particles, presumably elemental S^0, cover the spring sediment. Cultivation-based most probable number counts revealed microaerophilic iron(II)-oxidizers and sulphide-oxidizers to represent the largest fraction of iron- and sulphur-metabolizers in the spring, coexisting with less abundant iron(III)-reducers, sulphate-reducers and phototrophic and nitrate-reducing iron(II)-oxidizers. 16S rRNA gene 454 pyrosequencing showed sulphide-oxidizing *Thiothrix* species to be the dominating genus, supporting the results from our cultivation-based assessment. Collectively, our results suggest that anaerobic and microaerophilic iron- and sulphur-metabolizers could have coexisted in oxygenated ferro-sulphidic transition zones of late Archean and Proterozoic oceans, where they would have sustained continuous cycling of iron and sulphur compounds.

KEYWORDS
Fe-S cycles, Fe-S microbial community, mineralized alpine spring

1 | INTRODUCTION

Knowing the identity and composition of ancient microbial communities is vital to shed light onto the most compelling questions about the history of life, including the impact of rising oxygen levels in Earth's atmosphere and oceans on life's diversification. However, our understanding is incomplete as the remains of ancient metabolisms in the form of microfossils are rarely found in the rock record and also because the interpretation of chemical fingerprints in ancient rocks is challenging due to diagenetic alteration and/or metamorphic overprinting (Klein, 2005; Koeksoy, Halama, Konhauser, & Kappler, 2016).

The majority of Precambrian oceans were dominantly anoxic and ferruginous (rich in iron(II) (Poulton & Canfield, 2011)), and the bulk ocean presumably remained like this until the later Neoproterozoic (1.0–0.5 Ga) (Canfield et al., 2008; Planavsky et al., 2011). Hence, iron-metabolizing microorganisms probably played a key role in shaping the Precambrian biogeochemical environment before more complex eukaryotic life forms emerged and diversified. Striking evidence for the existence of such microorganisms early in Earth's history comes from banded iron formations (BIF), sedimentary rocks with a characteristic alternation of iron-rich and silica-rich layers that were deposited throughout the Archean (4.0–2.5 Ga) and Paleoproterozoic (2.5–1.6 Ga) (Bekker et al., 2010, 2014). For instance, iron isotope data in early Archean BIFs suggest the prevalence of phototrophic iron(II)-oxidizers by ca. 3.7 Ga (Czaja et al., 2013), while iron and neodymium isotopes together with rare Earth element analyses in late Archean BIFs suggest dissimilatory iron(III)-reducers to have recycled parts of continental iron in coastal sediments by ca. 2.5 Ga (Johnson, Beard, Klein, Beukes, & Roden, 2008; Li, Beard, & Johnson, 2015). Furthermore, microfossil data found in the Nuvvuagittuq supracrustal belt in Quebec, Canada, imply the very early existence of microaerophilic iron(II)-oxidizers already by 3.7 Ga, possibly even by 4.5 Ga (Dodd et al., 2017). Additional microfossil data from the Paleoproterozoic Jhamarkotra Formation, India (Crosby, Bailey, & Sharma, 2014), and iron isotope data in stromatolites from the Animikie basin of the Gunflint and Biwabik Formations, Canada and United States (Planavsky et al., 2009), indicate respective microorganisms to have flourished in slightly oxic surface zones of the ocean during high-oxygen intervals. Respective conditions are thought of having been widespread during the late Archean in form of oxygen oases (Olson, Kump, & Kasting, 2013), during the Paleoproterozoic Great Oxidation Event (GOE) (Holland, 2006) and throughout the Proterozoic (Planavsky et al., 2014; see Lyons, Reinhard, & Planavsky, 2014 for an overview).

Although these patches of information hint at the establishment of an ancient network of iron-metabolizers on Precambrian Earth, outstanding questions about their spatial distribution, community composition and interplay with metabolically different communities remain unsolved. In particular, their response to the expanding sulphate-reducing microbial community in coastal parts of the water column and in underlying sediments as a consequence of the enhanced delivery of dissolved sulphate to neritic ocean regions through increased oxidative weathering of terrestrial pyrite during high-oxygen intervals (Canfield, 1998) is uncertain. As a consequence, the accumulation of euxinic (sulphide-rich) waters by enhanced sulphate reduction rates and their expansion to intermediate-depth ocean regions of high biological productivity (Canfield, 1998; Poulton, Fralick, & Canfield, 2004, 2010; Reinhard, Raiswell, Scott, Anbar, & Lyons, 2009) likely triggered the proliferation of sulphur-oxidizers.

Deciphering the nature of the coexistence of iron- and sulphur-metabolizers in oxygenated ferro-euxinic transition zones of Precambrian oceans is essential to understand the biological and geochemical factors that controlled the extent of euxinic versus ferruginous conditions and that shaped the biogeochemical cycling of redox-active elements, including carbon, oxygen, iron and sulphur. As the available rock record data are insufficient to assemble a complete picture of ancient microbial community structure and activity, an alternative promising approach is the analysis of existing modern habitats that resemble conditions of relevant ancient settings (Koeksoy et al., 2016), such as Lake Matano (Crowe et al., 2008), Lake Pavin (Busigny et al., 2014), Lake La Cruz (Walter et al., 2014) and Kabuno Bay of Lake Kivu (Llirós et al., 2015). Accordingly, we present data from the iron- and sulphur-rich Arvadi Spring in the eastern Swiss Alps, which we posit to simulate the geochemical and microbial composition in shallow ferro-euxinic transition zones of late Archean and Proterozoic oceans during high-oxygen intervals. The main goals of this study were to (i) analyse the geochemical composition of the Arvadi Spring, (ii) to identify and quantify the key players of the iron- and sulphur-metabolizing bacterial communities and (iii) to predict late Archean and Proterozoic ocean geochemical and microbial community composition.

2 | MATERIALS AND METHODS

2.1 | Field site description

The highly mineralized Arvadi Spring is located in the Albula valley close to Bad Alvaneu (canton of Grisons, Switzerland) at an altitude of 928 m above sea level (46°40′17.4″N 9°39′18.8″E). It is situated in an alpine orogeny area comprising erosion of the Austroalpine overthrusts and the underlying Penninic rocks. Exposure of Jurassic oceanic crustal rocks and overlying sedimentary rocks resulted in the discharge of deeply circulating waters from lithologically variable rock units. The Arvadi Spring discharges from the crystalline rocks of the Silvretta nappe, which overlays carbonates and evaporitic gypsum, of which the latter is the source of sulphur species in the Arvadi Spring water (Strauss et al., 2016). The contemporaneous presence of both, iron and sulphur species, in the spring water results from a mixture of sulphur-rich water from a sulphide spring with iron-rich water from a second unknown subsurface water source. A scheme of the water flow system is provided in the supporting information file (Figure S1). Unfortunately, we had no access to the subsurface sources of the parental waters and hence cannot provide information on their geochemistry. The iron(II) and sulphide content of
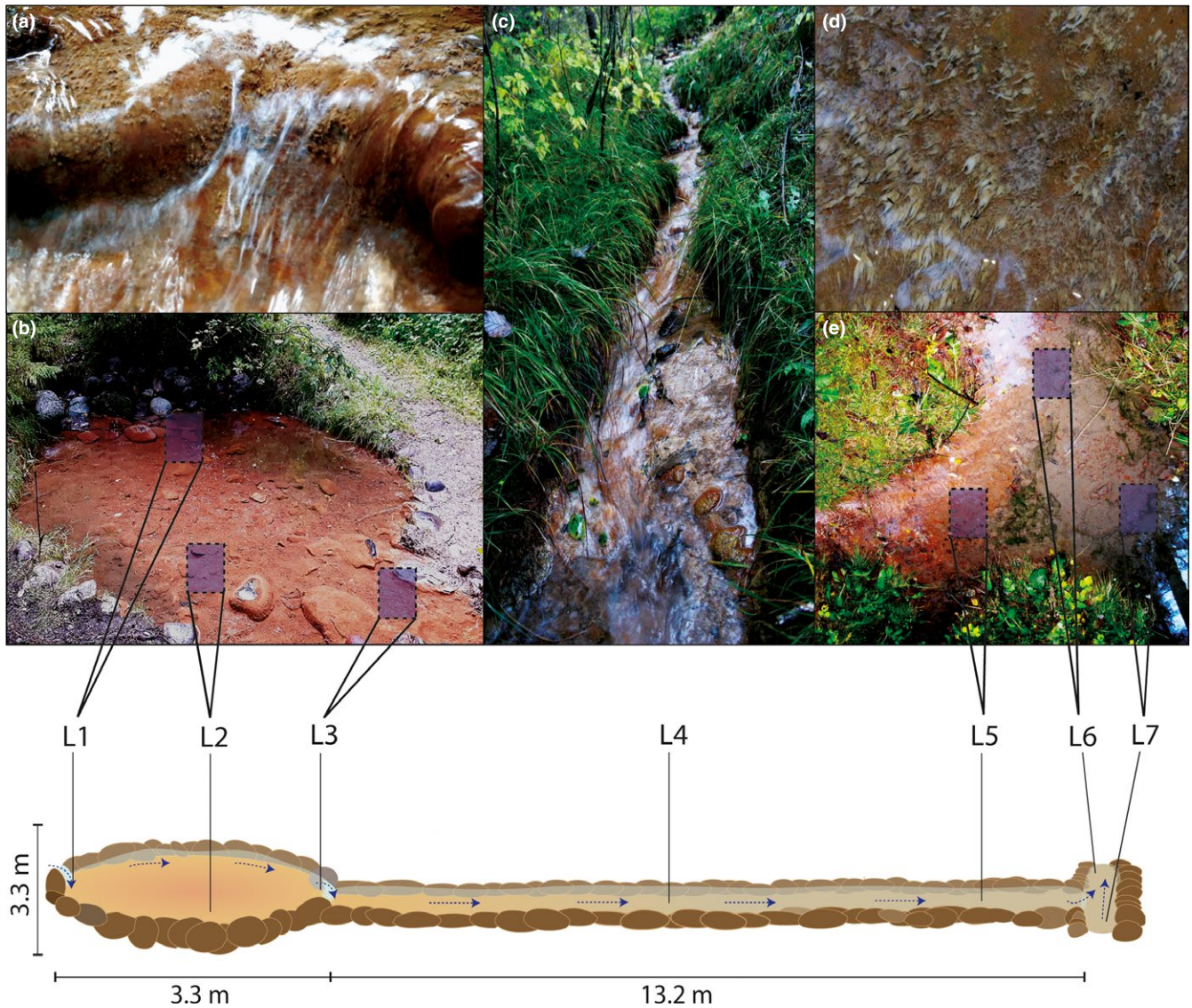
FIGURE 1 Schematic overview of the Arvadi Spring. Locations L1 and L2 are situated within the spring pond (b). L1 is located at the spring discharge and L3 at the transition of the water from the spring pond into the spring creek. Image (a) shows the transition of the spring pond to the creek at L3. Image (c) shows how the spring water flows via location L4 from the spring pond to location L5. Image (d) shows whitish biofilms grown at several locations within the spring creek. Image (e) shows how water from another creek (L7) gets mixed into Arvadi Spring water. The mixed water flows out into forestal area (L6)

sulphide- and iron(II)-rich water could be identified, however, at a connection point between the two different sourced waters in a mixing tunnel (CP2, see Figure S1) and were found to be 13.81 ± 1.33 μM and 8.00 ± 0.79 μM, respectively, at full oxygen saturation. From connection point 2, the intermixed water flows ca. 35 m downhill before it crops out into a manmade pond (the Arvadi Spring) with a diameter of 3.3 m and a water depth of ~20 cm (Figure 1). From the pond, the water flows into a creek of ca. 13 m length and converges with a second creek at 16.5 m distance from the spring discharge (Figure 1), which dilutes the Arvadi Spring water. The sediment of the spring pond is completely covered by soft reddish particles, which are overlain partly by fluffy whitish flocs that apparently have a lower density (Figure 2a, b). Rock surfaces in the spring pond are partly covered by white biofilms with filamentous elongations and partly by orange-brownish biofilm-like crusts. The soft red and white flocs are not present along the spring creek. Instead, the creek floor is covered by a thin orange-whitish crust.

2.2 | Field measurements of physical and chemical parameters and sampling

Major physical and chemical parameters (pH, temperature, oxygen content, electrical conductivity and salinity) were determined by in situ measurements at 7 locations in the spring water (Figure 1). Measurements were performed with a field multimeter (WTW, Multi 3430), containing an oxygen sensor (FDO®925, 0–200 ± 1.5% dissolved oxygen at 20°C), a conductivity electrode (TetraCon®925, conductivity range 1 μS/cm – 1 S/cm ± 1.5% of measured value)
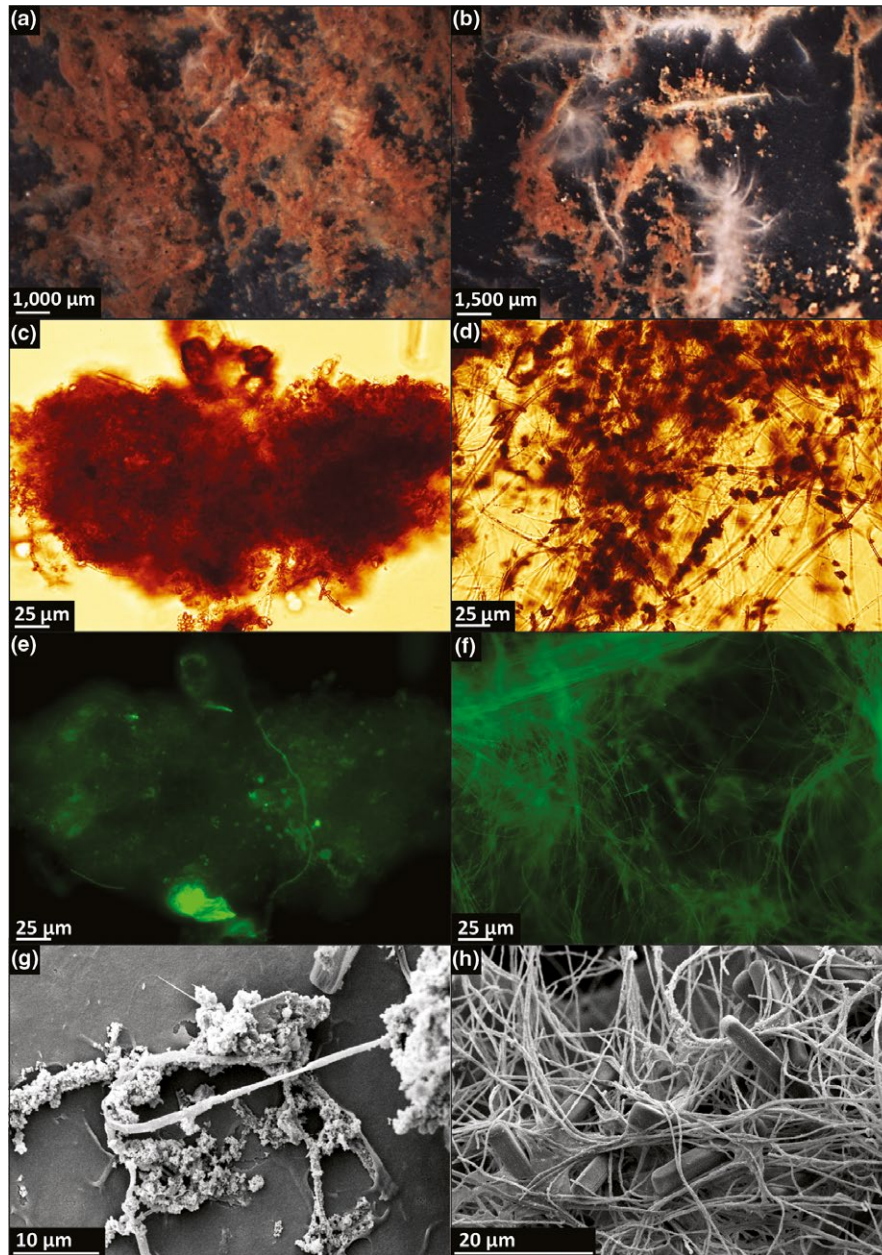
FIGURE 2 Binocular and microscopy images of red and white flocs and biofilm. Binocular images of a mixture of red and white flocs that cover the Arvadi Spring ground at L2 (a & b). Microscopy images of a red floc (c & e; taken from L2); red biofilm (g, taken from L3), white flocs (d & f, taken from L2) and white biofilm (h, taken from location 3). Binocular images (a & b) were taken at 10× magnification (A) and 15× magnification (B). Brightfield (c & d) and fluorescence mode images (e & f) were taken at 400× magnification. SEM images (g & h) were taken at 5,000× (g) and 2,000× (h) magnification

and a pH sensor (SenTix®, pH range 0.000–14.000 ± 0.004) with an additional temperature sensor. The pH and conductivity sensors were calibrated at room temperature according to manual instructions of the WTW Multi 3430 field multimeter. The pH sensor was calibrated with a three-point calibration using technical buffers at pH values 4.01, 7.00 and 10.00. The conductivity electrode was calibrated using a 0.01 mol/L KCl conductivity standard with a conductivity of 1,413 µS/cm at 25°C. The oxygen sensor is factory calibrated for the whole sensor lifetime with values stored in an internal memory chip within the sensor cap. The mean residence time of the

pond water was identified using NaCl as a tracer and conductivity measurements with the WTW TetraCon®925. The conductivity of the Arvadi Spring water at location 1 (L1, Figure 1) was doubled by dissolving the NaCl tracer in the spring water. The tracer was distributed homogeneously in the spring pond by stirring the pond water over the length of the experiment. The conductivity was logged until it returned to initial values.

Spring water for geochemical analyses was collected from two locations within the spring pond (L1 and L2, Figure 1). Samples were filtered to 0.45 µm in order to quantify major anions and

cations by ion chromatography, dissolved organic (DOC) and inorganic carbon (DIC) by a carbon analyser (highTOC, Elementar, Germany) and silica by Microwave Plasma-Atomic Emission Spectroscopy (MP-AES) (4200, Agilent Technologies, USA). Samples for Si quantification additionally were acidified with 2% HNO_3 prior to analyses. Water for bicarbonate analyses was sampled without headspace and titrated in the laboratory against 1 M HCl. To prevent oxidation of iron(II) by air-O_2 during sampling, water and red floc samples from L1 and L2 for iron quantification were directly added to 0.5 M HCl on site (Porsch & Kappler, 2011). Iron(II) and total iron were quantified in respective samples by the spectrophotometric ferrozine assay (Stookey, 1970) with a microplate reader (FlashScan 550, Analytic Jena, Germany). For the quantification of total iron, samples were added to 10% hydroxylamine hydrochloride (HAHCl) solution in order to reduce all iron(III) to iron(II). The iron(II) content in HAHCl reduced samples therefore represents total iron. Iron(III) concentrations were calculated by subtraction of iron(II) concentrations from total iron concentrations. Hydrogen sulphide was quantified in water samples from L1 and L2 by the methylene blue method after Cline (1969) with a photometer (FlashScan 550, Analytic Jena, Germany). Sulphide was prevented from oxidation by air-O_2 during sampling by fixation of samples in 2% (w/v) zinc-acetate solution (Cline, 1969).

2.3 | Mineralogical analyses

The mineralogy of the red flocs was identified by Mössbauer spectroscopy (Larese-Casanova, Kappler, & Haderlein, 2012). Precipitates were collected at L2 (Figure 1) and stored without headspace at 4°C in the dark prior to further treatment in the laboratory. Samples were dried by applying low pressure inside an anoxic glovebox (100% N_2) to avoid oxidation of potentially present redox-sensitive iron(II) minerals. The dried samples were ground in a mortar, filled in a flat cylinder-shaped plexiglas holder (with open top and an inner diameter of 1.5 cm) and fixed by a second smaller sample holder. For measurements, samples were inserted into a closed-cycle exchange gas cryostat (Janis cryogenics, USA). Spectra were recorded at 77 K and 4.2 K in transmission geometry using a constant acceleration drive system (WissEL GmbH, Germany). A ^{57}Co source embedded in a Rhodium matrix was used as gamma radiation source. The sample spectra were calibrated against a 7-µm-thick α-^{57}Fe foil at room temperature. The RECOIL software suite (University of Ottawa, Canada) was used for calibration and modelling of the spectra. The spectra were modelled using Voigt-based line shapes (Rancourt & Ping, 1991). The Lorentz half-width-half-maximum value (HWHM) was kept constant at 0.126 mm/s (determined from the minimum line width of the 3 and 4 peaks of the calibration foil) in the models. The Gauss' sigma (σ) parameter was used to account for line broadening until the fitting was reasonable. Sample spectra were analysed with respect to the centre shift (CS), shift/quadrupole splitting/(ε/QS) and hyperfine field (H).

2.4 | Microscopy

White and red flocs were sampled and stored at 4°C in the dark until analysis with a BMS 133 Trino binocular microscope (BMS Microscopes, NL). Samples for light microscopy were fixed in 2% paraformaldehyde. For fluorescence microscopy, samples were stained with SYTO9 stain (BacLight, Invitrogen, Carlsbad, CA) before analysis with a Leica DM 5500 B microscope (Leica Microsystems, Germany). Biofilm samples were fixed in 2.5% glutaraldehyde in the field to preserve biotic structures for Scanning Electron Microscopy (SEM) (Schädler, Burkhardt, & Kappler, 2008). The samples were then transported on ice and in the dark back to the laboratory where they were stored in a cold room overnight. The next day, samples were prepared on TEM grids or on glass slides, both pretreated with polylysine. The TEM grids were dipped into the preserved samples and then taken through a dehydration series consisting of 30%, 70%, 95% and 100% ethanol (with the samples being immersed for ca. 5 s in each solution) and 2 final steps with hexamethyldisilazane before samples were left to air dry. Samples were prepared on glass slides by first adding a droplet of sample onto the slide, after which excess liquid was pipetted away and each of the solutions in the dehydration series above was added to the glass slide and left for 10–15 min before being exchanged. Finally, all samples were placed on aluminium stubs with carbon tape and sputter-coated with platinum (6–8 nm, SCD005, BAL-TEC, Liechtenstein, 35 mm working distance, 30 mA, 60 s). SEM micrographs were recorded with a secondary electron detector of a Leo Model 1450VP SEM (Carl Zeiss SMT AG, Germany) operated at 7 kV and 6 mm working distance.

2.5 | Quantification of cell abundance by Most Probable Number (MPN) counts

Red and white flocs were collected separately from each location (L1 and L2; Figure 1) and stored without headspace at 4°C in the dark prior to the experiment. The red flocs were used for MPN enumerations of iron-metabolizers, while white flocs were used for MPN counts of sulphur-metabolizers after Oblinger and Koburger (Oblinger & Koburger, 1975; Straub, Kappler, & Schink, 2005). First, red and white flocs were homogenized separately. A 10^{-1} dilution was prepared by the addition of approximately 1 g wet weight of red flocs to 9 ml of freshwater (FW) medium and 1 g wet weight of white flocs to 9 ml of basal mineral (BM) medium, respectively (for detailed description of media composition, see SI). Starting with the 10^{-1} dilution, a 10-fold dilution series was prepared by sample transfer in a 1:10 ratio up to a dilution of 10^{-12}. The dilutions were used as inoculum for MPN experiments. Anaerobic iron- and sulphur-metabolizers were cultivated in anoxic growth media with selective additives, as listed below (Hegler, Posth, Jiang, & Kappler, 2008; Straub et al., 2005). Microaerophilic iron(II)- and sulphide-oxidizers were cultivated in gradient tubes after Emerson and Floyd (2005). Both types of MPN experiments were conducted as described by Laufer et al. (2016).

Iron-metabolizers were cultivated in FW medium amended with 30 mM $NaHCO_3$. Phototrophic iron(II)-oxidizers were cultivated with 10 mM $FeCl_2$ as iron(II) source and 5 mM Na_2MoO_4 to inhibit growth of sulphate-reducers. Nitrate-reducing iron(II)-oxidizers were cultivated in FW medium amended with 10 mM $FeCl_2$, 5 mM Na_2MoO_4, 4 mM $NaNO_3$ and 0.5 mM Na-acetate. Iron(III)-reducers were cultivated in FW medium amended with 5 mmol/L ferrihydrite as iron(III) source, 5 mM Na-acetate and 5 mM Na-lactate.

Phototrophic sulphide-oxidizers (purple and green sulphur bacteria as well as nonsulphur bacteria) were cultivated in BM medium amended with 30 mM $NaHCO_3$. BM medium for nonsulphur bacteria contained 0.1 mM Na_2S, 5 mM Na-acetate, 5 mM succinic acid and 5 mM maleic acid and had a final pH of 6.8. BM medium for purple sulphur bacteria was amended with 1.2 mM Na_2S and was adjusted to a final pH of 7.6. BM medium for green sulphur bacteria contained 2.5 mM Na_2S and was adjusted to a pH of 6.8. Nitrate-reducing sulphide-oxidizers were cultivated in BM medium amended with 1 mM $NaNO_3$, 1 mM Na_2S, 0.5 mM Na-acetate and 30 mM $NaHCO_3$.

Sulphate-reducers were cultivated in BM medium amended with 30 mM Na_2SO_4, 1 mM Na_2S and 10 mM Na-acetate. Microaerophiles were cultivated in gradient tubes prepared with Modified Wolfe's Mineral Medium (MWMM) (see SI) containing an iron(II) bottom plug in case of iron(II)-oxidizers, while gradient tubes for sulphide-oxidizers contained a Na_2S bottom layer.

Generally, anoxic MPN deep-well plates and MPN gradient tubes were evaluated visually for positive growth due to a colour change in test wells and tubes, either from (i) light greenish or colourless to orange-brownish indicating the presence of iron(III) (oxyhydr)oxide precipitates and thus iron(II) oxidation or (ii) from reddish to black indicating the precipitation of ferrous sulphides or mixed-valent iron(II)/iron(III) minerals and thus iron(III) reduction or (iii) from colourless to blackish indicating precipitation of ferrous sulphides and thus sulphate reduction or (iv) from colourless to purple indicating growth of purple (non-)sulphur bacteria or (v) from colourless to greenish indicating growth of green (non-)sulphur bacteria. In case of no visible colour change as it was the case for nitrate-reducing sulphide-oxidizers, growth was evaluated by sampling of the test wells and subsequent quantification of sulphide.

2.6 | DNA extraction, 454 pyrosequencing of 16S rRNA gene amplicons & sequence analyses

Sediment samples for DNA extraction and subsequent 454 pyrosequencing were collected from L2 (pond) and L5 (creek) (Figure 1). DNA was extracted from each sample with the Powersoil® DNA Isolation Kit (MoBio Laboratories, Carlsbad, CA, USA). DNA quality and quantity were determined spectrophotometrically using NanoDrop™ (ND 2000, PEQLAB biotechnology GmbH, Germany). Bacterial 16S rRNA genes were amplified using primers 27F (5′-AGAGTTTGATCMTGGCTCAG-3′, (Lane, 1991)) and 534R (5′-ATTACCGCGGCTGCTGGC-3′, (Liu, Lozupone, Hamady, Bushman, & Knight, 2007)) targeting the variable regions V1-V3 (507 bp). Both primers contained Roche 454 pyrosequencing barcodes. Primer

27F and 534R contained Roche 454-pyrosequencing adaptor sequences A and B, respectively. PCR was performed on each DNA extract in duplicate using the FastStart High Fidelity PCR System (Roche Diagnostics, Rotkreuz, Switzerland). PCR products were pooled in equal amounts. The amplified DNA was quantified using the Quant-iT™ PicoGreen® dsDNA assay kit (Life Technologies, Carlsbad, CA, USA) and a QuantiFluor®-ST fluorometer (Promega, Madison, WI, USA). 454 pyrosequencing was performed on a Roche GS Junior Sequencer (454 Life Sciences, Branford, CT, USA) according to the manufacturer's instructions for amplicon sequencing. Amplicon reads have been deposited in the NCBI Sequence Read Archive (accession number: SRP124992, bioproject: PRJNA417005).

Curation of the obtained sequencing data including quality control, sequence alignment and sequence classification was performed using the software package MOTHUR, version 1.35.1 (Schloss et al., 2009). Pyrosequencing noise including primer dimers, single base errors and PCR chimeras were removed with the MOTHUR-implemented algorithms PyroNoise (Quince et al., 2009) and UCHIME (Edgar, Haas, Clemente, Quince, & Knight, 2011). Sequences shorter than 200 bp and homopolymers longer than 8 bp were removed from the data set. All remaining high-quality sequences were aligned against the SILVA SSU Ref rRNA database (v119) (Pruesse et al., 2007) and preclustered with the single linkage algorithm at a threshold of 2% (Huse, Welch, Morrison, & Sogin, 2010). Sequences were assigned to operational taxonomic units (OTUs) based on 3% genetic distance using the average neighbour algorithm (Schloss & Westcott, 2011). Sequence classification was performed using the Naïve Bayesian Classifier (Wang, Garrity, Tiedje, & Cole, 2007) and the SILVA SSU rRNA reference database with a minimum bootstrap confidence cut-off value of 60%. Random subsampling was performed prior to alpha diversity analyses to normalize the data set to the sample with the lowest number of reads. Rarefaction curves, richness estimators (Chao1, ACE) and diversity indices (Shannon diversity, Simpson diversity) were calculated based on 3% genetic distance using MOTHURs implementation DOTUR (Schloss & Handelsman, 2005).

3 | RESULTS

3.1 | Geochemical composition of the Arvadi Spring water

Geochemical parameters were constant in the spring pond (locations L1, L2, L3; Figure 1; Table S1), as well as over the creek length with increasing distance from the spring discharge (locations L4, L5, L6; Figure 1; Table S1). Differences were observed at location L7, which is in the second creek and not the Arvadi Spring (Figure 1). The spring water in the pond had a circumneutral pH and a temperature of 7.0 to 7.3°C (Table 1). The water was saturated with oxygen (337.5 ± 1.3 µM, average ± standard deviation, $n = 3$, Table 1) but still contained dissolved iron(II) and sulphide at concentrations of 17.2 ± 2.8 µM and 2.5 ± 0.2 µM ($n = 5$, Table 1), respectively. Dissolved iron(III) was not detected in the spring water. The average

TABLE 1 Geochemical parameters in the Arvadi Spring pond water and approximations for respective parameters in late Archean and Proterozoic oceans from the literature

	Arvadi Spring Pond	Late Archean and Proterozoic ocean (surface)
T [°C]	7.2 ± 0.1	20–70[a,b]
pH	8.0 ± 0.0	6.5–8.5[c,d]
O_2 [μM]	337.5 ± 1.3	1–10 in late Archean oxygen oases[e]
		0.2 in mid-Proterozoic[f]
		>1 in Paleoproterozoic[g]
Salinity [‰]	0.7	35–70[h]
HCO_3^- [mM]	4.5 ± 0.0	~70[c]
Sulphate [mM]	8.3 ± 0.0	~0.08 for the late Archean[i]
		1.0–4.5 for the Paleo- and Mesoproterozoic[j,k]
Sulphide [μM]	2.5 ± 0.3	n.a.
Fe(II) [μM]	17.2 ± 2.8	40–120 in Archean oceans[k]
		<100 in Proterozoic oceans[l]
$SiO_{2(aq)}$ [μM]	134.3 ± 4.4	670–2,200[m]

Notes. Values for the Arvadi Pond are average ± standard deviation for *n* = 3 (L1–L3, see also Supporting information Tables S1 and S2). [a]Pinti (2005); [b]Robert and Chaussidon (2006); [c]Grotzinger and Kasting (1993); [d]Halevy and Bachan (2017); [e]Olson et al. (2013); [f]Tang, Shi, Wang, and Jiang (2016); [g]Hardisty et al. (2014); [h]Knauth (2005); [i]Jamieson, Wing, Farquhar, and Hannington (2013); [j]Canfield, Farquhar, and Zerkle (2010); [k]Kah, Lyons, and Frank (2004); [l]Canfield (2005); [l]Planavsky et al. (2011); [m]Konhauser, Lalonde, Amskold, and Holland (2007).

concentrations of the main anions and cations in the spring pond (L1-L3, Table S2; Table S3, *n* = 3) were sulphate (8.3 ± 0.1 mM), magnesium (3.2 ± 0.0 mM) and calcium (7.0 ± 0.0 mM). Total carbon was quantified at 50.9 ± 0.3 mg/L, of which 1.3 ± 0.7 mg/L was DOC (*n* = 3, Table S4). The bicarbonate content of the spring water was 4.5 ± 0.0 mM (*n* = 3, Table 1). Silica was quantified at 134.3 ± 4.4 μM in the spring pond water (*n* = 6, Table 1). On the basis of the conductivity measurements, which reflected the loss of the NaCl spike from the pond water, the mean residence time of the spring water in the pond was 16 min.

3.2 | Structure and composition of precipitates

The spring pond ground was completely covered by red floc precipitates partly overlain by whitish flocs (Figure 2a, b). Light microscopy showed the red floc material to be bulky and densely packed (Figure 2c), while white flocs consisted of filaments interspersed with smaller nodule structures (Figure 2d). Staining of the red and white flocs with SYTO9, a nucleic acid dye, indicated that both types of flocs consisted mainly of biotic structures (Figure 2e, f). SEM analyses of red and white biofilm samples recovered from rock surfaces at L3 (Figure 1d) revealed similar results as the microscopic analyses of red and white floc samples. The red biofilm contained mainly bulky and heterogeneous structures (Figure 2g) that were similar to the
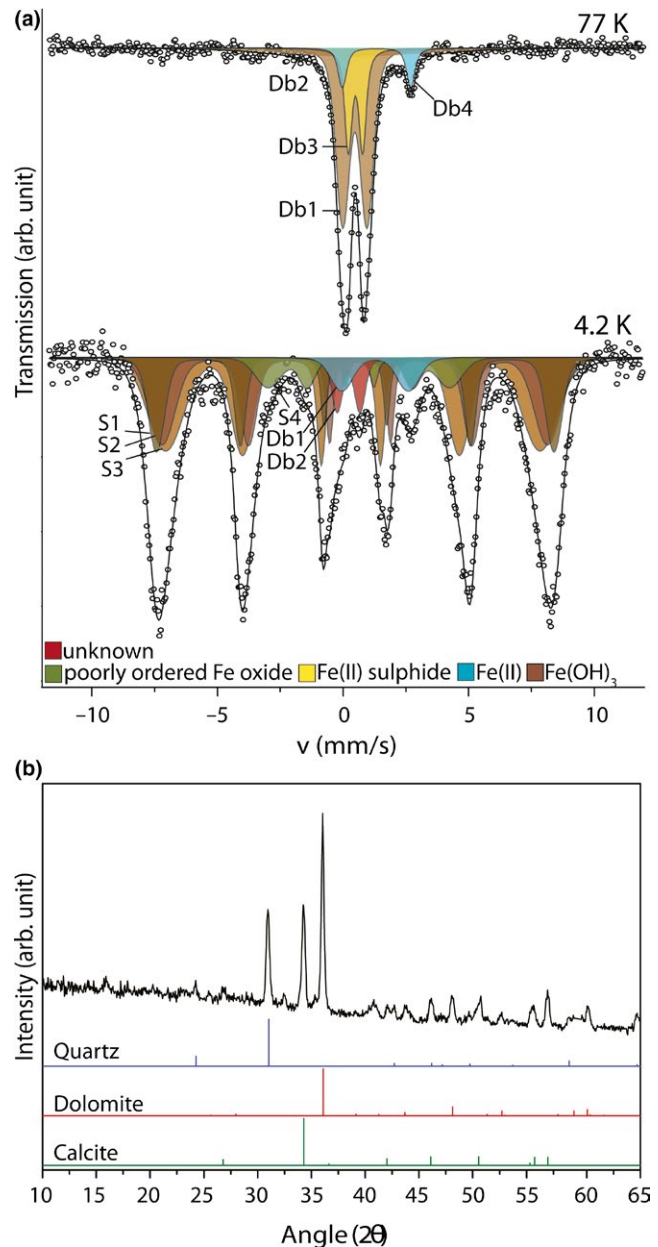
FIGURE 3 Mössbauer spectra obtained at 77 K and 4.2 K (a) and X-ray diffractograms (b) of red flocs

red floc morphology, whereas the white biofilm rather consisted of a web of filamentous structures (Figure 2h), as found in white flocs.

Quantification of the iron(II):iron(III) ratios in red flocs by the spectrophotometric ferrozine assay after acidic dissolution revealed iron(III) to be the dominant redox state, although the relative amounts varied between samples from L1 and L2. Red flocs from L1 had 77.0 ± 2.2% (average ± standard deviation, *n* = 5) iron(III) and a lower amount of iron(II) of 23.1 ± 2.2%. By contrast, red flocs from L2 contained 55.0 ± 3.7% and 45.0 ± 3.7% of iron(III) and iron(II), respectively.

Analysis by μXRD revealed the crystalline part of the red flocs to be dominated by quartz, calcite and dolomite (Figure 3). The

Mössbauer spectrum collected at 77K is best fitted by three doublets corresponding to paramagnetic iron phases with an additional phase having broad quadrupole splitting indicating the partial onset of magnetic ordering. The narrow paramagnetic doublet at 77K (Figure 3; CS = 0.5 mm/s; QS = 0.6 mm/s (see Table S5)) can potentially correspond to a number of mineral phases, such as lepidocrocite or iron(II) sulphides, including mono- and disulphides such as pyrrhotite and pyrite (Jeandey, Oddou, Mattei, & Fillion, 1991; Montano & Seehra, 1976). The 4.2K spectrum is dominated by several magnetically ordered sextets in addition to two doublets (Figure 3). The sextets are characteristic for poorly crystalline iron(III) (oxyhydr)oxide phases, and large inner-line broadening suggests an association with organic matter (Eusterhues et al., 2008; Shimizu et al., 2013). The wide paramagnetic doublet at 4.2K (Figure 3; CS = 1.3 mm/s; QS = 2.7 mm/s (see Table S5)) corresponds to an iron(II) phase, that could be either vivianite, green rust, siderite or even sorbed iron(II) (Domes et al., 1986). Based on the fitting of the spectrum collected at 4.2K, the calculated iron(II):iron(tot) ratio in the sample is 0.169.

3.3 | Microbial community composition and abundance of iron- and sulphur-metabolizers

The abundance of iron- and sulphur-metabolizing bacteria in red and white flocs was quantified by MPN counts (Figure 4). Microaerophilic sulphide-oxidizers were most abundant at L1 and L2, with 2.47×10^5 and 2.40×10^5 cells/g in the white flocs, respectively, followed by microaerophilic iron(II)-oxidizers with 2.47×10^4 and 2.40×10^4 cells/g in the red flocs. Anaerobic iron- and sulphur-metabolizers were quantified at lower abundances, with the lowest abundance among phototrophic iron(II)-oxidizers (6.03×10^1 and 5.26×10^2 cells/g red flocs), nitrate-reducing iron(II)-oxidizers (3.14×10^3 and 2.98×10^2 cells/g red flocs) and sulphate-reducers (3.05×10^2 and 2.40×10^2 cells/g white flocs). Iron(III)-reducers were the most abundant anaerobes among the iron- and sulphur-metabolizers with 2.47×10^3 and 2.97×10^4 cells/g red flocs). MPN numbers could not be determined for phototrophic and nitrate-reducing sulphide-oxidizers as only very few tubes inoculated for purple (non-)sulphur bacteria were positive and did not show a clear trend or growth for green (non-)sulphur bacteria and nitrate-reducing sulphide-oxidizers.

Of 454 pyrosequencing of bacterial 16S rRNA genes revealed that the Arvadi Spring pond and creek sediments contained diverse bacterial communities with 213 genera identified in total (Table S6). The most abundant phyla in both samples were Proteobacteria (57.8% and 59.0% rel. sequence abundance, respectively), Bacteroidetes (17.8% and 14.8% rel. sequence abundance, respectively) and Cyanobacteria (9.5% and 9.9% rel. sequence abundance; Figure 5a). On the genus level, the samples were dominated by *Thiothrix* (14.0% and 17.2% rel. sequence abundance, respectively), *Thiobacillus* (4.1% and 5.9%, respectively) and *Gemmobacter* (3.3% and 2.5%, respectively) (Figure 5b). Genera with relative sequence abundances below 1% were summarized as 'Other' and made up 17.5% and 19.2% of the total community, respectively. This group included
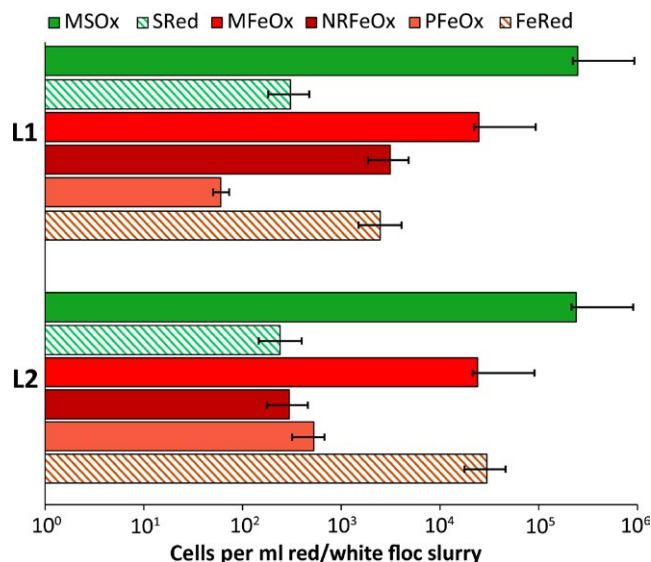

FIGURE 4 MPNs of iron- and sulphur-metabolizers in red and white flocs at locations L1 and L2: microaerophilic sulphide-oxidizers (MSOx), sulphate-reducers (SRed), microaerophilic (MFeOx), nitrate-reducing (NRFeOx) and phototrophic iron(II)-oxidizers (PFeOx) as well as iron(III)-reducers (FeRed). The error bars indicate upper and lower limits of the 95% confidence intervals for the estimates

various genera known to comprise iron- and sulphur-metabolizers such as *Acidiferrobacter*, *Acidithiobacillus*, *Acidovorax*, *Albidiferax*, *Desulfathirabdium*, *Desulfocapsa*, *Ferrithrix*, *Nitrospira*, *Sideroxydans*, *Sulfuricella*, *Sulfuricurvum*, *Sulfuritalea* and *Sulfurospirillum* (Table S6). Rarefaction analyses indicated that sampling did not fully recover the total estimated diversity (Figure S2). Richness estimators (Table S7) further suggested that the observed richness covered on average 57%–72% of the estimated total bacterial richness in the pond and creek samples. In general, the observed and estimated richness (based on Chao1 and ACE richness estimators) were higher in the pond compared to the creek sample. Diversity indices (Shannon and Simpson) suggested the pond and creek samples to be diverse to a similar extent.

4 | DISCUSSION

The Arvadi Spring is characterized by O_2 saturation, low concentrations of iron(II) and sulphide, considerable amounts of sulphate and high light availability. Figure 6 shows a model for biogeochemical iron and sulphur cycling in the Arvadi Spring that we hypothesize to apply to ferro-euxinic intermixed transition zones along redox interfaces of Proterozoic surface ocean waters and possibly also of late Archean oxygen oases during high-oxygen intervals (Figure 6b, Table 1). We evaluated iron(II)- and sulphide-consuming and -producing processes and identified the present geochemical iron and sulphur species in the Arvadi Spring to determine the factors that limit iron(II) and sulphide bioavailability, aiming to better
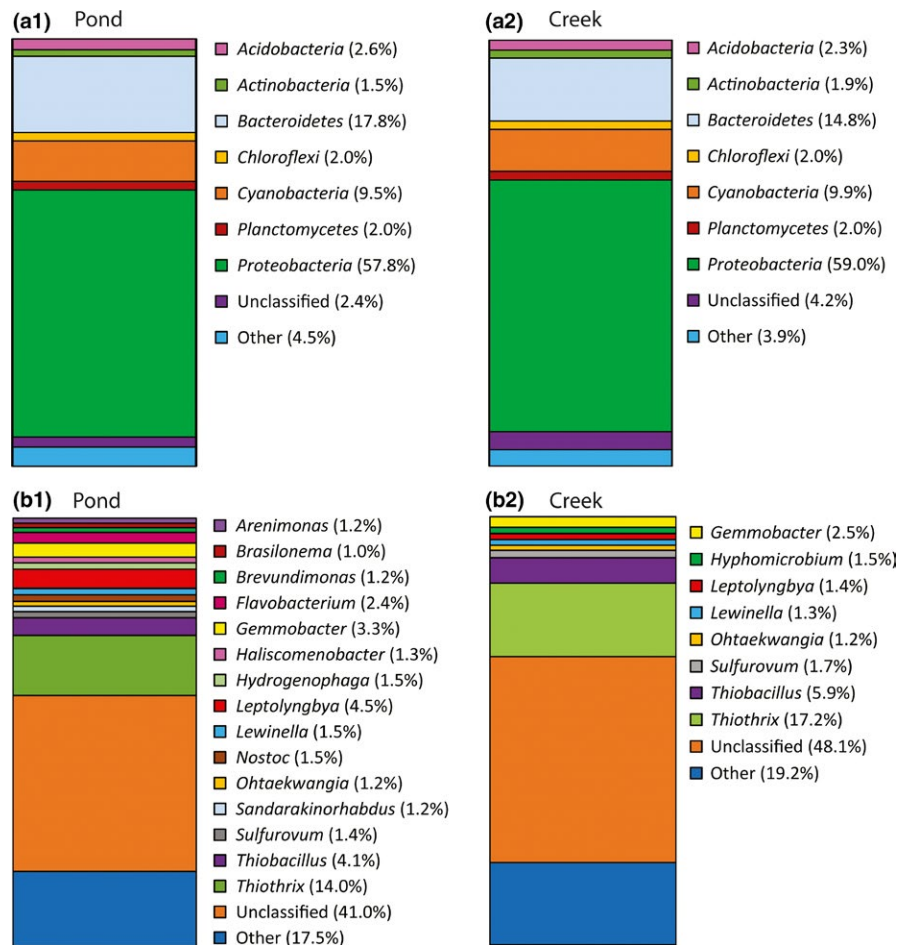
FIGURE 5 Taxonomic identity and relative sequence abundance of bacterial 16S rRNA genes on the class (a) and genus level (b) in Arvadi Spring pond and creek. For detailed information, see Supporting information Table S6

understand Precambrian biogeochemical iron- and sulphur-cycling under high-oxygen conditions.

4.1 | Iron(II)- and sulphide-producing and -consuming biogeochemical processes in the Arvadi Spring

Under full oxygenation and at the circumneutral pH of the Arvadi Spring water, dissolved iron(II) is expected to become oxidized abiotically by O_2 within minutes (Millero, Sotolongo, & Izaguirre, 1987a; Pham & Waite, 2008). As we found microaerophilic, phototrophic and nitrate-reducing iron(II)-oxidizing microorganisms to colonize Arvadi Spring red flocs, we conclude that a significant fraction of the total iron(II) budget is consumed by their metabolic processes (Figure 6a). The low but constant steady-state concentration of total dissolved iron(II) that we quantified (17.2 μM) is likely the result of a balance between its different sources and sinks. A certain fraction of dissolved iron(II) likely stems from dissimilatory iron(III) reduction, while iron(II) may also be formed by abiotic iron(III) reduction processes including photoreduction of ligand-bound iron(III) (Barbeau, Rue, Bruland, & Butler, 2001), the abiotic reaction of O_2 with ligand-bound or dissociated iron(III) (Rush & Bielski, 1985) or iron(III) reduction coupled to abiotic sulphide oxidation (Lohmayer, Kappler, Lösekann-Behrens, & Planer-Friedrich, 2014;

Yao & Millero, 1996). The initial concentration of iron(II) introduced to the Arvadi Spring pond together with the iron(II) from reductive processes may be sufficient to avoid being completely consumed by abiotic and biotic oxidation processes during the mean water residence time of 16 min in the pond, leaving residual iron(II) in solution. Other reasons for the low but stable iron(II) concentrations may be the presence of humic ligands that can stabilize iron(II) (Hopwood, Statham, Skrabal, & Willey, 2015; Statham, Jacobson, & Van Den Berg, 2012) and the large amounts of sulphate in the Arvadi water that can retard the abiotic oxidation of iron(II) to a certain extent (Millero, 1985).

Microbial reduction in gypsum-derived sulphate that is present in large amounts in the Alpine orogeny is the major source of sulphide in the Arvadi Spring (Strauss et al., 2016). Compared to iron(II), sulphide is oxidized abiotically by O_2 much more slowly, that is, on the order of hours to days (Luther et al., 2011; Millero, Hubinger, Fernandez, & Garnett, 1987b). Hence, we expect the majority of aqueous sulphide to be oxidized microbially and not abiotically, as the water residence time in the pond is only 16 min. Our MPN and 16S rRNA gene sequence analyses suggest microaerophilic sulphide-oxidizers to play a major role in sulphide consumption within the Arvadi Spring, as *Thiothrix*, a genus representative of aerobic sulphide-oxidizers (Nielsen, De Muro, & Nielsen, 2000), was identified to dominate the Arvadi Spring microbial community.
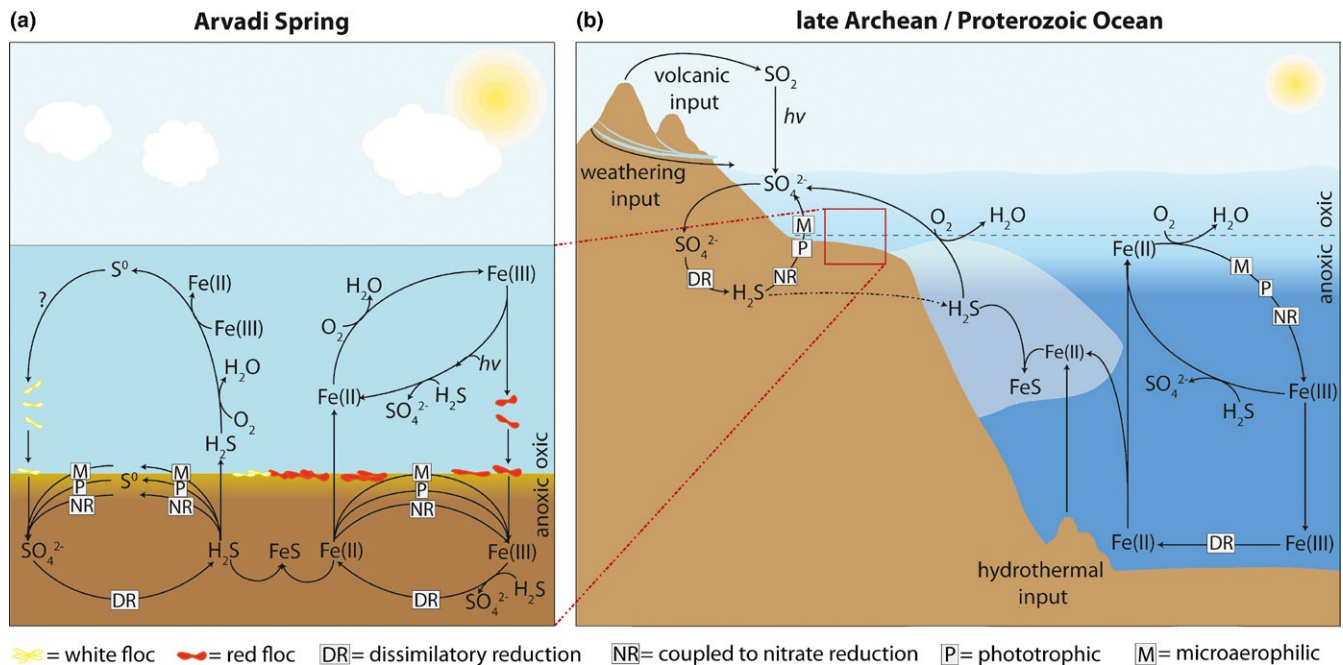
= white floc ••• = red floc DR = dissimilatory reduction NR = coupled to nitrate reduction P = phototrophic M = microaerophilic

FIGURE 6 Simplified model of biogeochemical iron and sulphur cycling in the Arvadi Spring and its relevance for late Archean and Proterozoic ocean iron and sulphur cycling. a: Abiotic oxidation reactions in the Arvadi Spring pond occur mainly in the oxic water, producing S^0 and iron(III) that are further metabolized in the spring sediment. Red and white flocs are potential products of abiotic and biotic iron(II) and sulphide oxidation. White flocs are expected to contain S^0, while red flocs consist of iron(III) minerals. These compounds get metabolized by microbial processes (indicated by squares, see legend) at the oxic–anoxic sediment surface and in anoxic deeper sediment layers. The same biotic and abiotic redox processes are also expected to occur in red and white floc precipitates (not shown). b: The Arvadi Spring model possibly represents conditions near the redoxcline in late Archean and Proterozoic oceans (see red dashed lines and box), where enough light and/or oxygen were available to support phototrophic and aerobic microbial processes and where sulphide-rich and iron(II)-rich waters were mixed with oxygenated surface waters. The iron cycle on the right-hand side of the image probably also contemporaneously took place in neritic sediments (not shown). The grey shaded area indicates euxinic water masses formed by dissimilatory sulphate reduction

The observed growth of *Thiothrix*-like filamentous biofilms (Bland & Staley, 1978) at several locations (Figure 1a, d) gives hints on respective microorganisms to flourish in the Arvadi Spring. Minor sulphide portions may be metabolized by phototrophic and nitrate-reducing sulphide-oxidizers (Figure 6a) that were indicated to be part of the Arvadi Spring community based on 16S rRNA gene sequencing data (phototrophic sulphide-oxidizers in the families *Chlorobiaceae*, *Chromatiaceae* and *Chloroflexi* and nitrate-reducing sulphide-oxidizers in the genera *Arcobacter* and *Thiobacillus*, respectively; see Table S6). However, we could neither determine taxonomic identity on the strain level nor whether respective microorganisms actually perform phototrophic and nitrate-reducing sulphide-oxidation in situ. Furthermore, as we could not quantify the (probably low) abundance of respective microorganisms by MPN counts and do not have evidence for their metabolic activity in the Arvadi Spring, the overall role that phototrophic and nitrate-reducing sulphide-oxidizers play in the Arvadi Spring requires further investigations in the future.

We expect elemental sulphur (S^0)—a key intermediate during sulphur metabolism that is stored intra- or extracellularly by sulphide-oxidizing microorganisms such as *Thiothrix* spp.

(Nielsen et al., 2000)—to be present in Arvadi Spring solids, in particular in white floc precipitates (Figure 6a) and whitish biofilms (Figure 1d). However, additional mineralogical and speciation experiments are required to decipher the identity of sulphur intermediates and related processes such as S^0 disproportionation or S^0 oxidation in Arvadi Spring precipitates in order to uncover their relative importance on the overall sulphur budget in the Arvadi Spring and, by inference, in parts of ferro-euxinic transition zones along redox interfaces and chemoclines of shallow Proterozoic and late Archean ocean waters during high-oxygen intervals.

The coexistence of iron(II) and sulphide at the μM concentration range in the Arvadi Spring water likely applies to respective ancient habitats (Figure 6b). However, respective values should not be taken as representative for the bulk of ancient seawater, as anoxia was the prevailing feature of Precambrian oceans. The (reductive) sources of iron(II) and sulphide probably exceeded their sinks (microaerophilic/abiotic oxidation and precipitation) during anoxic intervals, with iron(II) and sulphide concentrations presumably having peaked at higher concentrations (e.g., iron(II) reaching 40–120 μM as suggested for Archean oceans (Canfield, 2005)).

4.2 | Iron redox speciation in the Arvadi Spring and iron(II) bioavailability for iron(II)-oxidizing microorganisms

Fe(III) is poorly soluble at neutral pH and dissolved iron(III) only occurs as colloidal or ligand-bound (complexed) iron(III) (Cornell & Schwertmann, 2003). As we could not detect dissolved iron(III) in the spring water, iron(III) complexes must play a relatively minor role in the Arvadi Spring water, with most iron(III) precipitating directly after formation as iron(III) minerals. Wet-chemical extraction followed by ferrozine analyses and Mössbauer spectroscopy clearly showed red flocs to consist of poorly crystalline iron(III) (oxyhydr) oxides similar to ferrihydrite (see Table S5, Figure 3). This is in accordance with the common observation of ferrihydrite formation through abiotic iron(II) oxidation by O_2 or by microaerophilic iron(II)-oxidizers in other cold-water springs with circumneutral pH (Hegler, Lösekann-Behrens, Hanselmann, Behrens, & Kappler, 2012; Jambor & Dutrizac, 1998; James & Ferris, 2004; Konhauser, Kappler, & Roden, 2011). Thus, red flocs probably form through a combination of biotic and abiotic iron(II) oxidation (Figure 6a).

The Mössbauer spectra (Table S5) and ferrozine analyses showed iron(II) to be present in red flocs, which likely stems from dissimilatory iron(III) reduction proceeding in red flocs in addition to iron(II) oxidation based on our MPN results. Interestingly, the iron(II) content of 45% as determined in red flocs from location L2 using acidic extraction and the spectrophotometric ferrozine assay contradicts our Mössbauer results which suggest an iron(II):iron(tot) ratio of 16.9% in the sample. This discrepancy may be due to abiotic reduction in iron(III) by sulphide that is released during acidic extraction and thus made available for iron(III) reduction. Also, sulphide produced by potentially more intensely ongoing sulphate reduction in closely associated white flocs from L2 (see MPN results) may be responsible for the observed discrepancy.

Generally, we suggest the iron(II) in red flocs to be consumed by iron(II)-oxidizers that colonize red flocs. However, the bioavailability of iron(II) in red flocs depends on its speciation as for instance the bioavailability of mineral-bound iron(II) depends on mineral solubility (Kappler & Newman, 2004; Zhao, Campbell, & Wilkinson, 2016). Iron(II) in more stable minerals is less bioavailable, as for instance, pyrite (solubility product (K_{SP}) = $10^{-16.4 \pm 1.2}$ (Davison, 1991)) was shown not to be metabolized by phototrophic iron(II)-oxidizers at neutral pH, whereas other iron(II) minerals (such as poorly crystalline FeS (K_{SP} = $10^{-2.95 \pm 0.1}$; (Davison, 1991)) or iron(II) carbonate (K_{SP} = $10^{-2.94 \pm 0.4}$; (Bénézeth, Dandurand, & Harrichoury, 2009)) with higher solubility were oxidized (Kappler & Newman, 2004). Intuitively, based on the presence of iron(II), sulphide and high carbonate content in the Arvadi Spring water, we considered the possibility that a fraction of the iron(II) in the red flocs occurs as iron(II) sulphide and as siderite minerals. Being highly reactive towards each other, iron(II) and sulphide precipitate as poorly crystalline ferrous sulphide if their concentrations reach supersaturation (Rickard & Luther, 2007) and transform further into more stable iron(II) sulphides (i.e., pyrite or pyrrhotite) (Rickard, 2006; Rickard & Luther,

2007). However, under the given Arvadi Spring water geochemistry and a calculated saturation index of −7.42 for amorphous FeS, such FeS mineral phases are unlikely to precipitate in the Arvadi Spring, although the formation of dissolved and/or colloidal FeS complexes and nanoparticulate higher crystalline FeS species such as mackinawite at hotspots where higher sulphide and iron(II) are present (for example in deeper sediments) cannot be excluded (Luther & Rickard, 2005). Our Mössbauer results indicate the narrow paramagnetic doublet at 77 K to potentially account for an FeS phase, suggesting locally formed iron(II) and sulphide from iron(III) and sulphate reduction that proceed in close association in red and white flocs to reach supersaturation and hence to result in the formation of different FeS minerals at spatially restricted sites (Figure 6a). Our Mössbauer results further indicate siderite to be formed in the Arvadi Spring, which is in line with a calculated saturation index of 2.67 for siderite formation based on the Arvadi water geochemistry. As these conclusions are mostly based on theoretical considerations using the geochemical conditions in the Arvadi water, further investigation of the iron- (and sulphur-) speciation in red and white flocs is required to understand the actual mineral identity and the mechanisms behind their formation.

Our observations suggest that dissolved iron(III) was probably absent in Precambrian ocean margins with intermixed ferro-euxinic-oxic waters, except in low abundances of ligand-bound or colloidal forms. Moreover, the iron(III) minerals formed by microaerophilic and abiotic iron(II) oxidation were likely poorly crystalline and ferrihydrite-like. The formed iron(III) particles may have been similar in their structure and composition to Arvadi Spring red flocs and probably were colonized by microorganisms, in particular by iron-metabolizers, during and after sinking to the ocean floor. These particles likely also contained ferrous minerals, which resulted from dissimilatory iron(III) reduction. Respective iron(II) phases could have included green rust (Halevy, Alesker, Schuster, Popovitz-Biro, & Feldman, 2017), as well as iron(II) sulphides that precipitated directly from the ferro-euxinic surface ocean waters (Canfield, 1998; Lyons, 2008). These iron sulphides likely settled together with red floc-like particles and transformed over time to more stable iron(II) sulphides (e.g., pyrite).

4.3 | Adaptation of iron- and sulphur-metabolizers to Arvadi Spring's high O_2 content

Our results show the co-occurrence of phototrophic, nitrate-reducing and microaerophilic iron(II)-oxidizers and microaerophilic sulphide-oxidizers with dissimilatory iron(III)- and sulphate-reducers in an iron- and sulphur-rich environment. Based on bioturbation in the spring ground by movement of the prevalent macrobiota together with the apparently low density of red and white flocs and hence their subjection to water movement from the top, we assume intermixing of different sediment layers with red and white flocs to proceed over the whole year and hence the different metabolic types of microorganisms to co-occur in different ecological niches throughout the seasons (especially as our results were reproducible

with samples from different seasons, data not shown). Partial introduction of certain metabolic types of microorganisms from the ambient water is inevitable and hence may have a minor impact on the observed composition.

The dense microbial networks associated with Arvadi Spring red and white flocs (Figure 2e, f) contain heterotrophic aerobic respiring bacteria (*Gemmobacter*, *Hydrogenophaga* and *Pseudomonas*, see Table S6). Oxygen consumption by these microbes, alongside abiotic O_2-consuming reactions, for example, abiotic O_2-dependent sulphide and iron(II) oxidation can create microoxic or anoxic microniches in otherwise oxic environments (Brune, Frenzel, & Cypionka, 2000). Based on the significant numbers of anaerobic and microaerophilic Fe- and S-metabolizing microorganisms that we found in MPN experiments, we suggest anoxic and microoxic microniches to be present in the Arvadi Spring and that such microsites should be analysed in future experiments for example using O_2-, Fe- or E_h-microelectrodes. Based on the lower abundance of anaerobes compared to microaerophiles, the high O_2 content in the Arvadi Spring is probably limiting obligate anaerobes in their growth and activity. Additionally, it has to be considered that potentially some anaerobes could have been washed from other locations to the spots that were sampled and based on our data it is not possible to fully distinguish between scenarios where the different types of organisms really co-occur in association with each other or whether they just co-occur in the collected sample.

Aerobic microorganisms are unlikely to have dominated the bulk of the late Archean and Proterozoic ocean microbiome as anoxia was the prevailing feature by that time with the exception of settings that were similar to the Arvadi Spring. Our finding of a predominance of microaerophiles over anaerobes therefore should only be understood as a likely scenario for redox-stratified ocean waters in paleoshorelines during high-oxygen intervals. In respective settings, O_2-tolerant and even O_2-dependent lifestyles may have evolved and became widespread. We suggest that in settings similar to the Arvadi Spring, phototrophic and nitrate-reducing iron(II)-oxidizers would not have been abundant, if not generally metabolically inactive. Nitrate may have been scarce in Precambrian oceans (Fennel, Follows, & Falkowski, 2005; Godfrey & Falkowski, 2009) as it is the case in the Arvadi Spring, whereby a recent study by Michiels et al. (2017) on N-cycling in ferruginous Kabuno Bay implies the contrast, suggesting significant contribution of nitrate-reducing iron(II)-oxidizers to global Proterozoic N-retention. Further, the redox stratification of the Precambrian ocean with the first appearance of oxic conditions and the accompanying formation of oxy- and chemoclines may have rearranged the spatial distribution of microbial communities, with microaerophiles presumably having colonized topmost oxic (and photic) layers. They likely coexisted with phototrophs, but competing for iron(II), phototrophs may have decreased in their abundance in oxic intervals at respective sites.

4.4 | Implications for Fe-S-cycling in ferro-euxinic transition zones of shallow late Archean and Proterozoic ocean waters

The present study provides new insights from a modern iron(II)-, sulphide- and O_2-rich model habitat regarding the potential network of iron- and sulphur-metabolizing microorganisms in shallow ferro-euxinic transition zones of Precambrian oceans that were influenced by the presence of O_2 in the water and atmosphere. The Arvadi Spring data implies the iron- and sulphur-metabolizing microbial community that presumably coexisted in respective ancient sites to have been dominated by microaerophiles. However, considering a higher prevalence of anoxia for the bulk of Precambrian oceans, anaerobic iron- and sulphur-metabolizers presumably would have still been dominating over microaerophiles on the global level. Comparing the observed morphology in red and white flocs (Figure 2) to microfossil structures found in the rock record that are interpreted as remains of early microorganisms (Schopf et al., 2015) we suggest similar microbial networks to have colonized mineral particles that settled from ferro-euxinic intermixed surface waters of the late Archean and Proterozoic ocean.

Collectively, the Arvadi Spring helps us to understand how O_2 consumption by aerobic microorganisms and production of reduced compounds by anaerobic respiring microorganisms (e.g., iron(II) and sulphide) could have affected the abundance, activity and survival of anaerobic members of the upper, oxygenated ancient ocean metabolic network by forming anoxic niches. In particular, for the interpretation of signatures found in the rock record, the Arvadi Spring can help to understand which biotic and abiotic processes resulted in the isotope composition that was preserved in the rock record (Strauss et al., 2016), to decipher the identity of the primary minerals prior to diagenesis and to know the morphology of the microbial community that exists under envisaged conditions prior to preservation in form of microfossils. To further improve our model and our understanding of the metabolic network of iron- and sulphur-metabolizing microorganisms, we need to know the factors controlling the interrelation and competition of iron- and sulphur-metabolizers with abiotic reactions in the Arvadi Spring. This includes understanding the relative importance of different metabolic types of iron- and sulphur-metabolizers by determining rates of the individual processes. To evaluate the impact of changing redox conditions on the microbial community activities, controlled laboratory microcosm experiments are required, which include variations in O_2 availability and in iron(II) and sulphide concentrations. The quantification of microbial versus abiotic rates of iron(II) and sulphide oxidation, as well as rates of iron(III) and sulphate reduction in the Arvadi Spring by iron- and sulphur-metabolizers, is a prerequisite to decipher biogeochemical iron and sulphur cycling in detail. Only by unravelling the response of a living microbial community to postulated geochemical frameworks, we can reconstruct the ancient biosphere and geosphere as a whole.

ORCID

Andreas Kappler http://orcid.org/0000-0002-3558-9500

REFERENCES

Barbeau, K., Rue, E., Bruland, K., & Butler, A. (2001). Photochemical cycling of iron in the surface ocean mediated by microbial iron (III)-binding ligands. *Nature*, *413*, 409–413. https://doi.org/10.1038/35096545

Bekker, A., Planavsky, N. J., Krapež, B., Rasmussen, B., Hofmann, A., Slack, J. F., ... Konhauser, K. O. (2014). Iron formations: Their origins and implications for ancient seawater chemistry. In H. Holland, & K. Turekian (Eds.), *Treatise on geochemistry* (pp. 561–628). Waltham, MA: Elsevier Ltd. https://doi.org/10.1016/B978-0-08-095975-7.00719-1

Bekker, A., Slack, J. F., Planavsky, N., Krapež, B., Hofmann, A., Konhauser, K. O., & Rouxel, O. J. (2010). Iron formation: The sedimentary product of a complex interplay among mantle, tectonic, oceanic, and biospheric processes. *Economic Geology*, *105*, 467–508. https://doi.org/10.2113/gsecongeo.105.3.467

Bénézeth, P., Dandurand, J. L., & Harrichoury, J. C. (2009). Solubility product of siderite (FeCO$_3$) as a function of temperature (25–250°C). *Chemical Geology*, *265*, 3–12. https://doi.org/10.1016/j.chemgeo.2009.03.015

Bland, J. A., & Staley, J. T. (1978). Observations on the biology of Thiothrix. *Archives of Microbiology*, *117*, 79–87. https://doi.org/10.1007/BF00689355

Brune, A., Frenzel, P., & Cypionka, H. (2000). Life at the oxic-anoxic interface: Microbial activities and adaptations. *Federation of European Microbiological Societies Microbiology Reviews*, *24*, 691–710.

Busigny, V., Planavsky, N. J., Jézéquel, D., Crowe, S., Louvat, P., Moureau, J., ... Lyons, T. W. (2014). Iron isotopes in an Archean ocean analogue. *Geochimica et Cosmochimica Acta*, *133*, 443–462. https://doi.org/10.1016/j.gca.2014.03.004

Canfield, D. E. (1998). A new model for Proterozoic ocean chemistry. *Nature*, *396*, 450–453. https://doi.org/10.1038/24839

Canfield, D. E. (2005). The early history of atmospheric oxygen: Homage to Robert M. Garrels. *Annual Review of Earth and Planetary Sciences*, *33*, 1–36. https://doi.org/10.1146/annurev.earth.33.092203.122711

Canfield, D. E., Farquhar, J., & Zerkle, A. L. (2010). High isotope fractionations during sulfate reduction in a low-sulfate euxinic ocean analog. *Geology*, *38*, 415–418. https://doi.org/10.1130/G30723.1

Canfield, D. E., Poulton, S. W., Knoll, A. H., Narbonne, G. M., Ross, G., Goldberg, T., & Strauss, H. (2008). Ferruginous conditions dominated later Neoproterozoic deep-water chemistry. *Science*, *321*, 949–952. https://doi.org/10.1126/science.1154499

Cline, J. D. (1969). Spectrophotometric determination of hydrogen sulfide in natural waters. *Limnology and Oceanography*, *14*, 454–458. https://doi.org/10.4319/lo.1969.14.3.0454

Cornell, R. M., & Schwertmann, U. (2003). *The iron oxides: Structure, properties, reactions, occurrences and uses*. Weinheim, Germany: Wiley-VCH. https://doi.org/10.1002/3527602097

Crosby, C. H., Bailey, J. V., & Sharma, M. (2014). Fossil evidence of iron-oxidizing chemolithotrophy linked to phosphogenesis in the wake of the Great Oxidation Event. *Geology*, *42*, 1015–1018. https://doi.org/10.1130/G35922.1

Crowe, S.A., Jones, C., Katsev, S., Magen, C., O'neill, A.H., Sturm, A., ... Sundby, B. (2008). Photoferrotrophs thrive in an Archean Ocean analogue. *Proceedings of the National Academy of Sciences*, *105*, 15938–15943. https://doi.org/10.1073/pnas.0805313105

Czaja, A. D., Johnson, C. M., Beard, B. L., Roden, E. E., Li, W. Q., & Moorbath, S. (2013). Biological Fe oxidation controlled deposition of banded iron formation in the ca. 3770 Ma Isua Supracrustal Belt (West Greenland). *Earth and Planetary Science Letters*, *363*, 192–203. https://doi.org/10.1016/j.epsl.2012.12.025

Davison, W. (1991). The solubility of iron sulphides in synthetic and natural waters at ambient temperature. *Aquatic Sciences*, *53*, 309–329. https://doi.org/10.1007/BF00877139

Dodd, M. S., Papineau, D., Grenne, T., Slack, J. F., Rittner, M., Pirajno, F., ... Little, C. T. S. (2017). Evidence for early life in Earth's oldest hydrothermal vent precipitates. *Nature*, *543*, 60–64. https://doi.org/10.1038/nature21377

Domes, H., Leupold, O., Nagy, D. L., Ritter, G., Spiering, H., Molnár, B., & Szücs, I. S. (1986). Mössbauer study of short range order in frozen aqueous solutions of Fe(ClO$_4$)$_2$. *The Journal of Chemical Physics*, *85*, 7294–7300. https://doi.org/10.1063/1.451367

Edgar, R. C., Haas, B. J., Clemente, J. C., Quince, C., & Knight, R. (2011). UCHIME improves sensitivity and speed of chimera detection. *Bioinformatics*, *27*, 2194–2200. https://doi.org/10.1093/bioinformatics/btr381

Emerson, D., & Floyd, M. M. (2005). Enrichment and isolation of iron-oxidizing bacteria at neutral pH. *Methods in Enzymology*, *397*, 112–123. https://doi.org/10.1016/S0076-6879(05)97006-7

Eusterhues, K., Wagner, F. E., Häusler, W., Hanzlik, M., Knicker, H., Totsche, K. U., ... Schwertmann, U. (2008). Characterization of ferrihydrite-soil organic matter coprecipitates by X-ray diffraction and Mössbauer spectroscopy. *Environmental Science & Technology*, *42*, 7891–7897. https://doi.org/10.1021/es800881w

Fennel, K., Follows, M., & Falkowski, P. G. (2005). The co-evolution of the nitrogen, carbon and oxygen cycles in the Proterozoic ocean. *American Journal of Science*, *305*, 526–545. https://doi.org/10.2475/ajs.305.6-8.526

Godfrey, L. V., & Falkowski, P. G. (2009). The cycling and redox state of nitrogen in the Archean ocean. *Nature Geoscience*, *2*, 725–729. https://doi.org/10.1038/ngeo633

Grotzinger, J. P., & Kasting, J. F. (1993). New constraints on Precambrian ocean composition. *The Journal of Geology*, *101*, 235–243. https://doi.org/10.1086/648218

Halevy, I., Alesker, M., Schuster, E. M., Popovitz-Biro, R., & Feldman, Y. (2017). A key role for green rust in the Precambrian oceans and the genesis of iron formations. *Nature Geoscience*, *10*, 135–139. https://doi.org/10.1038/ngeo2878

Halevy, I., & Bachan, I. (2017). The geologic history of seawater pH. *Science*, *355*, 1069–1071. https://doi.org/10.1126/science.aal4151

Hardisty, D. S., Lu, Z., Planasky, N. J., Bekker, A., Philippot, P., Zhou, X., & Lyons, T. W. (2014). An iodine record of Paleoproterozoic surface ocean oxygenation. *Geology*, *42*, 619–622. https://doi.org/10.1130/G35439.1

Hegler, F., Lösekann-Behrens, T., Hanselmann, K., Behrens, S., & Kappler, A. (2012). Influence of seasonal and geochemical changes on the geomicrobiology of an iron carbonate mineral water spring. *Applied and Environmental Microbiology*, *78*, 7185–7196. https://doi.org/10.1128/AEM.01440-12

Hegler, F., Posth, N. R., Jiang, J., & Kappler, A. (2008). Physiology of phototrophic iron(II)-oxidizing bacteria: Implications for modern and ancient environments. *Federation of European Microbiological*

Societies Microbiology Ecology, 66, 250–260. https://doi.org/10.1111/j.1574-6941.2008.00592.x

Holland, H. D. (2006). The oxygenation of the atmosphere and oceans. *Philosophical Transactions of the Royal Society B: Biological Sciences*, 361, 903–915. https://doi.org/10.1098/rstb.2006.1838

Hopwood, M. J., Statham, P. J., Skrabal, S. A., & Willey, J. D. (2015). Dissolved iron(II) ligands in river and estuarine water. *Marine Chemistry*, 173, 173–182. https://doi.org/10.1016/j.marchem.2014.11.004

Huse, S. M., Welch, D. M., Morrison, H. G., & Sogin, M. L. (2010). Ironing out the wrinkles in the rare biosphere through improved OTU clustering. *Environmental Microbiology*, 12, 1889–1898. https://doi.org/10.1111/j.1462-2920.2010.02193.x

Jambor, J. L., & Dutrizac, J. E. (1998). Occurrence and constitution of natural and synthetic ferrihydrite, a widespread iron oxyhydroxide. *Chemical Reviews*, 98, 2549–2585. https://doi.org/10.1021/cr970105t

James, R. E., & Ferris, F. G. (2004). Evidence for microbial-mediated iron oxidation at a neutrophilic groundwater spring. *Chemical Geology*, 212, 301–311. https://doi.org/10.1016/j.chemgeo.2004.08.020

Jamieson, J. W., Wing, B. A., Farquhar, J., & Hannington, M. D. (2013). Neoarchean seawater sulphate concentrations from sulphur isotopes in massive sulphide ore. *Nature Geoscience*, 6, 61–64. https://doi.org/10.1038/ngeo1647

Jeandey, C., Oddou, J. L., Mattei, J. L., & Fillion, G. (1991). Mössbauer investigation of the pyrrhotite at low temperature. *Solid State Communications*, 78, 195–198. https://doi.org/10.1016/0038-1098(91)90282-Z

Johnson, C. M., Beard, B. L., Klein, C., Beukes, N. J., & Roden, E. E. (2008). Iron isotopes constrain biologic and abiologic processes in banded iron formation genesis. *Geochimica et Cosmochimica Acta*, 72, 151–169. https://doi.org/10.1016/j.gca.2007.10.013

Kah, L. C., Lyons, T. W., & Frank, T. D. (2004). Low marine sulphate and protracted oxygenation of the Proterozoic biosphere. *Nature*, 431, 834–838. https://doi.org/10.1038/nature02974

Kappler, A., & Newman, D. K. (2004). Formation of Fe(III)-minerals by Fe(II)-oxidizing photoautotrophic bacteria. *Geochimica et Cosmochimica Acta*, 68, 1217–1226. https://doi.org/10.1016/j.gca.2003.09.006

Klein, C. (2005). Some Precambrian banded iron-formations (BIFs) from around the world: Their age, geologic setting, mineralogy, metamorphism, geochemistry, and origin. *American Mineralogist*, 90, 1473–1499. https://doi.org/10.2138/am.2005.1871

Knauth, L. P. (2005). Temperature and salinity history of the Precambrian ocean: Implications for the course of microbial evolution. *Paleogeography, Paleoclimatology, Paleoecology*, 219, 53–69. https://doi.org/10.1016/j.palaeo.2004.10.014

Koeksoy, E., Halama, M., Konhauser, K. O., & Kappler, A. (2016). Using modern ferruginous habitats to interpret Precambrian banded iron formation deposition. *International Journal of Astrobiology*, 15, 205–217. https://doi.org/10.1017/S1473550415000373

Konhauser, K. O., Kappler, A., & Roden, E. E. (2011). Iron in microbial metabolisms. *Elements*, 7, 89–93. https://doi.org/10.2113/gselements.7.2.89

Konhauser, K. O., Lalonde, S. V., Amskold, L., & Holland, H. D. (2007). Was there really an Archean phosphate crisis? *Science*, 315, 1234. https://doi.org/10.1126/science.1136328

Lane, D. J. (1991). 16S/23S rRNA sequencing. In E. Stackebrandt, & M. Godfellow (Eds.), *Nucleic acid techniques in bacterial systematics* (pp. 115–175). New York, NY: Wiley.

Larese-Casanova, P., Kappler, A., & Haderlein, S. B. (2012). Heterogeneous oxidation of Fe(II) on iron oxides in aqueous systems: Identification and controls of Fe(III) product formation. *Geochimica et Cosmochimica Acta*, 91, 171–186. https://doi.org/10.1016/j.gca.2012.05.031

Laufer, K., Byrne, J. M., Glombitze, C., Schmidt, C., Jorgensen, B. B., & Kappler, A. (2016). Anaerobic microbial Fe(II) oxidation and Fe(III) reduction in coastal marine sediments controlled by organic carbon content. *Environmental Microbiology*, 18, 3159–3174. https://doi.org/10.1111/1462-2920.13387

Li, W., Beard, B. L., & Johnson, C. M. (2015). Biologically recycled continental iron is a major component in banded iron formations. *Proceedings of the National Academy of Science*, 112, 8193–8198. https://doi.org/10.1073/pnas.1505515112

Liu, Z. Z., Lozupone, C., Hamady, M., Bushman, F. D., & Knight, R. (2007). Short pyrosequencing reads suffice for accurate microbial community analysis. *Nucleic Acids Research*, 35, e120. https://doi.org/10.1093/nar/gkm541

Llirós, M., García-Armisen, T., Darchambeau, F., Morana, C., Triadó-Margarit, X., Inceoğlu, Ö., … Crowe, S. A. (2015). Pelagic photoferrotrophy and iron cycling in a modern ferruginous basin. *Scientific Reports*, 5, 13803. https://doi.org/10.1038/srep13803

Lohmayer, R., Kappler, A., Lösekann-Behrens, T., & Planer-Friedrich, B. (2014). Sulfur species as redox partners and electron shuttles for ferrihydrite reduction by Sulfurospirillum deleyianum. *Applied and Environmental Microbiology*, 80, 3141–3149. https://doi.org/10.1128/AEM.04220-13

Luther, G. W., Findlay, A. J., Macdonald, D. J., Owings, S. M., Hanson, T. E., Beinart, R. A., & Girguis, P. R. (2011). Thermodynamics and kinetics of sulfide oxidation by oxygen: A look at inorganically controlled reactions and biologically mediated processes in the environment. *Frontiers in Microbiology*, 2, 62.

Luther, G. W., & Rickard, D. T. (2005). Metal sulfide cluster complexes and their biogeochemical importance in the environment. *Journal of Nanoparticle Research*, 7, 389–407. https://doi.org/10.1007/s11051-005-4272-4

Lyons, T. W. (2008). Ironing out ocean chemistry at the dawn of animal life. *Science*, 321, 923–924. https://doi.org/10.1126/science.1162870

Lyons, T. W., Reinhard, C. T., & Planavsky, N. J. (2014). The rise of oxygen in Earth's early ocean and atmosphere. *Nature*, 506, 307–315. https://doi.org/10.1038/nature13068

Michiels, C. C., Darchambeau, F., Roland, F. A., Morana, C., Lliros, M., García-Armisen, T., … Servais, P. (2017). Iron-dependent nitrogen cycling in a ferruginous lake and the nutrient status of Proterozoic oceans. *Nature Geoscience*, 10, 217–221. https://doi.org/10.1038/ngeo2886

Millero, F. J. (1985). The effect of ionic interactions on the oxidation of metals in natural waters. *Geochimica et Cosmochimica Acta*, 49, 547–553. https://doi.org/10.1016/0016-7037(85)90046-8

Millero, F. J., Hubinger, S., Fernandez, M., & Garnett, S. (1987b). Oxidation of H_2S in seawater as a function of temperature, pH, and ionic strength. *Environmental Science and Technology*, 21, 439–443. https://doi.org/10.1021/es00159a003

Millero, F. J., Sotolongo, S., & Izaguirre, M. (1987a). The oxidation kinetics of Fe(II) in seawater. *Geochimica et Cosmochimica Acta*, 51, 793–801. https://doi.org/10.1016/0016-7037(87)90093-7

Montano, P. A., & Seehra, M. S. (1976). Magnetism of iron pyrite (FeS_2) — a Mössbauer study in an external magnetic field. *Solid State Communications*, 20, 897–898. https://doi.org/10.1016/0038-1098(76)91300-4

Nielsen, P. H., De Muro, M. A., & Nielsen, J. L. (2000). Studies on the in situ physiology of Thiothrix spp. present in activated sludge. *Environmental Microbiology*, 2, 389–398. https://doi.org/10.1046/j.1462-2920.2000.00120.x

Oblinger, J. L., & Koburger, J. A. (1975). Understanding and teaching most probable number technique. *Journal of Milk and Food Technology*, 38, 540–545. https://doi.org/10.4315/0022-2747-38.9.540

Olson, S. L., Kump, L. R., & Kasting, J. F. (2013). Quantifying the areal extent and dissolved oxygen concentrations of Archean oxygen

oases. *Chemical Geology*, *362*, 35–43. https://doi.org/10.1016/j.chemgeo.2013.08.012

Pham, A. N., & Waite, T. D. (2008). Oxygenation of Fe(II) in natural waters revisited: Kinetic modeling approaches, rate constant estimation and the importance of various reaction pathways. *Geochimica et Cosmochimica Acta*, *72*, 3616–3630. https://doi.org/10.1016/j.gca.2008.05.032

Pinti, L. D. (2005). The origin and evolution of the oceans. In M. Gargaud, B. Barbier, H. Martin, & J. Reisse (Eds.), *Lectures in astrobiology* (pp. 83–112). Heidelberg, Germany: Springer. https://doi.org/10.1007/b10889

Planavsky, N. J., Mcgoldrick, P., Scott, C. T., Li, C., Reinhard, C. T., Kelly, A. E., ... Lyons, T. W. (2011). Widespread iron-rich conditions in the mid-Proterozoic ocean. *Nature*, *477*, 448–451. https://doi.org/10.1038/nature10327

Planavsky, N. J., Reinhard, C. T., Wang, X., Thomson, D., Mcgoldrick, P., Rainbird, R. H., ... Lyons, T. W. (2014). Low Mid-Proterozoic atmospheric oxygen levels and the delayed rise of animals. *Science*, *346*, 635–638. https://doi.org/10.1126/science.1258410

Planavsky, N., Rouxel, O., Bekker, A., Shapiro, R., Fralick, P., & Knudsen, A. (2009). Iron-oxidizing microbial ecosystems thrived in late Paleoproterozoic redox-stratified oceans. *Earth and Planetary Science Letters*, *286*, 230–242. https://doi.org/10.1016/j.epsl.2009.06.033

Porsch, K., & Kappler, A. (2011). Fe^{II} oxidation by molecular O$_2$ during HCl extraction. *Environmental Chemistry*, *8*, 190–197. https://doi.org/10.1071/EN10125

Poulton, S. W., & Canfield, D. E. (2011). Ferruginous conditions: A dominant feature of the ocean through Earth's history. *Elements*, *7*, 107–112. https://doi.org/10.2113/gselements.7.2.107

Poulton, S. W., Fralick, P. W., & Canfield, D. E. (2004). The transition to a sulphidic ocean ~1.84 billion years ago. *Nature*, *431*, 173–177. https://doi.org/10.1038/nature02912

Poulton, S. W., Fralick, P. W., & Canfield, D. E. (2010). Spatial variability in oceanic redox structure 1.8 billion years ago. *Nature Geoscience*, *3*, 486–490. https://doi.org/10.1038/ngeo889

Pruesse, E., Quast, C., Knittel, K., Fuchs, B. M., Ludwig, W. G., Peplies, J., & Glockner, F. O. (2007). SILVA: A comprehensive online resource for quality checked and aligned ribosomal RNA sequence data compatible with ARB. *Nucleic Acids Research*, *35*, 7188–7196. https://doi.org/10.1093/nar/gkm864

Quince, C., Lanzen, A., Curtis, T. P., Davenport, R. J., Hall, N., Head, I. M., ... Sloan, W. T. (2009). Accurate determination of microbial diversity from 454 pyrosequencing data. *Nature Methods*, *6*, 639–641. https://doi.org/10.1038/nmeth.1361

Rancourt, D., & Ping, J. (1991). Voigt-based methods for arbitrary-shape static hyperfine parameter distributions in Mössbauer spectroscopy. *Nuclear Instruments and Methods in Physics Research Section B: Beam Interactions with Materials and Atoms*, *58*, 85–97. https://doi.org/10.1016/0168-583X(91)95681-3

Reinhard, C. T., Raiswell, R., Scott, C., Anbar, A. D., & Lyons, T. W. (2009). A late Archean sulfidic sea stimulated by early oxidative weathering of the continents. *Science*, *326*, 713–716. https://doi.org/10.1126/science.1176711

Rickard, D. (2006). The solubility of FeS. *Geochimica et Cosmochimica Acta*, *70*, 5779–5789. https://doi.org/10.1016/j.gca.2006.02.029

Rickard, D., & Luther, G. W. (2007). Chemistry of iron sulfides. *Chemical Reviews*, *107*, 514–562. https://doi.org/10.1021/cr0503658

Robert, F., & Chaussidon, M. (2006). A paleotemperature curve for the Precambrian oceans based on silicon isotopes in cherts. *Nature*, *443*, 969–972. https://doi.org/10.1038/nature05239

Rush, J. D., & Bielski, B. H. (1985). Pulse radiolytic studies of the reaction of HO$_2$/O$_2^-$ with Fe(II)/Fe(III) ions. The reactivity of HO$_2$/O$_2^-$ with ferric ions and its implication on the occurrence of the Haber-Weiss

reaction. *The Journal of Physical Chemistry*, *89*, 5062–5066. https://doi.org/10.1021/j100269a035

Schädler, S., Burkhardt, C., & Kappler, A. (2008). Evaluation of electron microscopic sample preparation methods and imaging techniques for characterization of cell-mineral aggregates. *Geomicrobiology Journal*, *25*, 228–239. https://doi.org/10.1080/01490450802153462

Schloss, P. D., & Handelsman, J. (2005). Introducing DOTUR, a computer program for defining operational taxonomic units and estimating species richness. *Applied and Environmental Microbiology*, *71*, 1501–1506. https://doi.org/10.1128/AEM.71.3.1501-1506.2005

Schloss, P. D., & Westcott, S. L. (2011). Assessing and improving methods used in operational taxonomic unit-based approaches for 16S rRNA gene sequence analysis. *Applied and Environmental Microbiology*, *77*, 3219–3226. https://doi.org/10.1128/AEM.02810-10

Schloss, P. D., Westcott, S. L., Ryabin, T., Hall, J. R., Hartmann, M., Hollister, E. B., ... Weber, C. F. (2009). Introducing mothur: Open-source, platform-independent, community-supported software for describing and comparing microbial communities. *Applied and Environmental Microbiology*, *75*, 7537–7541. https://doi.org/10.1128/AEM.01541-09

Schopf, J. W., Kudryavtsev, A. B., Walter, M. R., Van Kranendonk, M. J., Williford, K. H., Kozdon, R., ... Flannery, D. T. (2015). Sulfur-cycling fossil bacteria from the 1.8-Ga Duck Creek Formation provide promising evidence of evolution's null hypothesis. *Proceedings of the National Academy of Sciences*, *112*, 2087–2092. https://doi.org/10.1073/pnas.1419241112

Shimizu, M., Zhou, J. H., Schroder, C., Obst, M., Kappler, A., & Borch, T. (2013). Dissimilatory reduction and transformation of ferrihydrite-humic acid coprecipitates. *Environmental Science and Technology*, *47*, 13375–13384. https://doi.org/10.1021/es402812j

Statham, P. J., Jacobson, Y., & Van Den Berg, C. M. G. (2012). The measurement of organically complexed Fe^{II} in natural waters using competitive ligand reverse titration. *Analytica Chimica Acta*, *743*, 111–116. https://doi.org/10.1016/j.aca.2012.07.014

Stookey, L. L. (1970). Ferrozine – A new spectrophotometric reagent for iron. *Analytical Chemistry*, *42*, 779–781. https://doi.org/10.1021/ac60289a016

Straub, K. L., Kappler, A., & Schink, B. (2005). Enrichment and isolation of ferric-iron- and humic-acid-reducing bacteria. *Methods in Enzymology*, *397*, 58–77. https://doi.org/10.1016/S0076-6879(05)97004-3

Strauss, H., Chmiel, H., Christ, A., Fugmann, A., Hanselmann, K., Kappler, A., ... Teichert, B. M. A. (2016). Multiple sulphur and oxygen isotopes reveal microbial sulphur cycling in spring waters in the Lower Engadin, Switzerland. *Isotopes in Environmental and Health Studies*, *52*, 75–93. https://doi.org/10.1080/10256016.2015.1032961

Tang, D., Shi, X., Wang, X., & Jiang, G. (2016). Extremely low oxygen concentration in mid-Proterozoic shallow seawater. *Precambrian Research*, *276*, 145–157. https://doi.org/10.1016/j.precamres.2016.02.005

Walter, X. A., Picazo, A., Miracle, M. R., Vicente, E., Camacho, A., Aragno, M., & Zopfi, J. (2014). Phototrophic Fe(II)-oxidation in the chemocline of a ferruginous meromictic lake. *Frontiers in Microbiology*, *5*, 713.

Wang, Q., Garrity, G. M., Tiedje, J. M., & Cole, J. R. (2007). Naive Bayesian classifier for rapid assignment of rRNA sequences into the new bacterial taxonomy. *Applied and Environmental Microbiology*, *73*, 5261–5267. https://doi.org/10.1128/AEM.00062-07

Yao, W. S., & Millero, F. J. (1996). Oxidation of hydrogen sulfide by hydrous Fe(III) oxides in seawater. *Marine Chemistry*, *52*, 1–16. https://doi.org/10.1016/0304-4203(95)00072-0

Zhao, C. M., Campbell, P. G. C., & Wilkinson, K. J. (2016). When are metal complexes bioavailable? *Environmental Chemistry, 13*, 425–433.

SUPPORTING INFORMATION

Additional supporting information may be found online in the Supporting Information section at the end of the article.